Sixth International Symposium on Turbulence and Shear Flow Phenomena
Seoul, Korea, 22-24 June 2009

LARGE EDDY SIMULATION OF A LEAN PREMIXED LOW SWIRL BURNER

Mohammad Irannezhad
Department of Applied Mechanics,
Chalmers University of Technology
SE-41296 Gothenburg, Sweden
mohammad.irannezhad@chalmers.se

Lars-Erik Eriksson
Department of Applied Mechanics,
Chalmers University of Technology
SE-41296 Gothenburg, Sweden
lee@chalmers.se

ABSTRACT

Flow filed and flame front dynamics of a low swirl burner are investigated using numerical tools. Large eddy simulation and a flame capturing combustion model are applied to predict the flow field and the flame structure on two different computational domains and the results are compared to experimental data in order to recognize the most important phenomena in flame stabilization and dynamics. Investigations show that the flame dynamics are resulted from the large scale turbulence generated at the inlet of the fuel/air mixture and physical results are only attainable if this turbulence is generated in simulations by some means.

INTRODUCTION

Lean premixed combustion has increasingly gained interest in recent years as an approach toward reduced NO_x emissions. However, lean blow off limit and the tendency of the dynamic flame to become unstable present technical challenges. Low swirl stabilized combustion concept is a rather new and promising design to stabilize lean premixed flames close to flammability limit. This enables the burner to work at lower temperatures, hence producing lowerNO_x emissions. In swirl stabilized combustion, the bluff body is substituted with a divergent swirling flow to aerodynamically provide the low velocity and recirculation regions where the flame can stabilize. Unlike conventional high swirl burners, the recirculation region is very weak in low swirl burners and the flame stabilization is not relied on flame anchoring by recirculation (Cheng et al., 2000). Several numerical studies have been conducted to simulate these reacting flows (Nogenmyr, 2008; Irannezhad and Eriksson, 2008), but the underlying physical processes and the stabilization mechanism are not yet well understood. Here, numerical tools are applied to further investigate the characteristics of the flow and combustion in these burners.

This work has been done within CeCoST (Center for Combustion Science and Technology) activities in a Swedish national research program, aiming at stable and clean combustion. The aim of this work is to improve and validate existing LES-based modeling tools for turbulent premixed combustion under swirl conditions and to use the developed numerical models to gain deeper understanding of premixed combustion processes. The experimental validation data is obtained in parallel in another project within CeCoST activities at Lund University (Petersson, 2007).

TEST CASE

The low swirl burner test rig simulated in this work is installed at Lund University and is based on the design described originally by Bédat and Cheng(1995). The four radial jets of the original design are replaced by eight swirler vanes to ensure a more symmetric flow and better reproducibility.

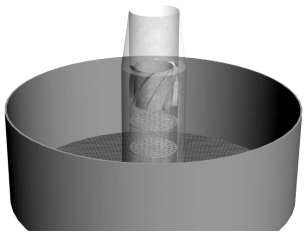

Figure 1: The experimental test rig showing the two perforated plates, swirler vanes/perforated plate, burner nozzle and the co-flow region.

Figure 2: The perforated-plate/swirler-vanes configuration shown inside the burner nozzle.

Figure 1 shows the burner experimental test rig, in which a constant mass flow of lean premixed methane/air mixture at equivalence ratio of 0.62 is blown into the $50mm$ diameter burner nozzle. First, the flow passes through two perforated plates which aim at providing a uniform flow across the entire nozzle diameter. Then the flow passes through a perforated-plate/swirler-vane configuration, figure 2, which is located approximately one diameter upstream of

the burner exit. This perforated plate and the eight swirler vanes encircling it, divide the flow into two regions: a near wall swirling flow and an axial core flow. The perforated plate also gives a pre-specified range of turbulence scales to the core flow. The burner nozzle is surrounded by a wide $0.35m/s$ axial co-flow to prevent disturbances from the surroundings as shown in figure 1. This configuration results in a detached flame stabilized in about one diameter downstream of the burner exit without any flame holders.

COMPUTATIONAL GRID

The computational domain adapted to the geometry does not contain the first two perforated plates and starts right after the perforated-plate/swirler-vanes configuration. The perforated plate and the swirler vanes are not included in the domain. It extends 10 diameters downstream of the burner exit in axial direction. In radial direction, the domain includes the co-flow region and spans out into the ambient (figure 3).

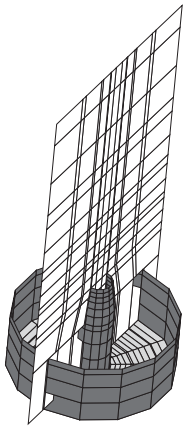

Figure 3: Computational domain, the grid lines shown do not represent the real grid lines.

The cells in the core of the cylindrical domain are Cartesian to avoid singularities at the centerline while the outer blocks are cylindrical. Simulations are performed on two block-structured grids, a coarse grid with around 750000 cells and a fine grid with around 6000000 cells, to investigate the grid resolution effects on the problem. Since the domain starts at the perforated-plate/swirler-vanes, figure 4, the velocity profile at this location needs to be set as boundary conditions.

NUMERICAL METHOD

The LES solver used to simulate the flow is an in-house code which has been successfully applied to a range of different problem areas, including gas turbine combustors, afterburners , ramjet combustors, jet noise predictions (Andersson et al., 2005), etc. The LES solver applies the Smagorinsky sub-grid scale model to solve the Favre-averaged Navier-Stokes equations including species transport equations. The flow is of low velocity and lies well within the incompressible limit, therefore preconditioning concept of Eriksson(1996) is used to efficiently solve this flow with the compressible solver. A cell-centered finite-volume scheme with explicit three-stage Runge-Kutta time stepping is used to integrate

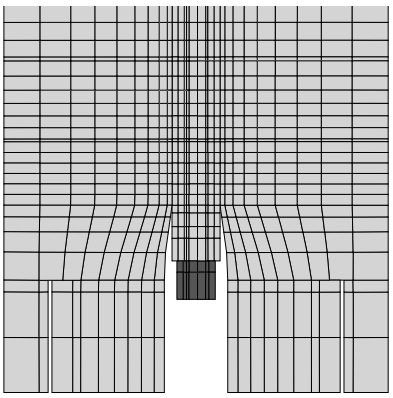

Figure 4: Center plane of the computational domain showing the start of the computational domain. The dark area is not included in the coarse and fine mesh simulations and is added when the perforated plate is added to the domain. The grid lines do not represent the real grid lines.

the equations in time. The convective flux is approximated with a third order accurate characteristic upwind scheme with low diffusion whereas a locally centered compact second order scheme approximates the diffusive flux.

The combustion model is based on a single reaction model,

$$Fu + s.O_2 \longrightarrow (1+s)Pr \tag{1}$$

where s is the stoichiometric ratio by weight ($s = 4$ for methane).

A flame speed correlation combustion model gives the effective reaction rate RR at each cell,

$$RR = \rho \cdot A_k \cdot Y^{(Fu)} \tag{2}$$

where ρ is density, $Y^{(Fu)}$ is the fuel mass fraction and A_k is the specific rate of fuel consumption given by

$$A_k = \begin{cases} \frac{C \cdot S_T^2}{\nu_{eff}} & \text{if } T > T_L \\ 0 & \text{if } T < T_L \end{cases} \tag{3}$$

where C is a dimensionless coefficient, T is the temperature and T_L is a threshold temperature below which all reactions are neglected. The turbulent flame speed S_T and the effective viscosity ν_{eff} are approximated as,

$$S_T = S_L + 2 \cdot \sqrt{k_{sgs}} \tag{4}$$

$$\nu_{eff} = \nu + \nu_{sgs} \tag{5}$$

where k is the sub-grid scale turbulent kinetic energy, ν is the laminar viscosity and ν_{sgs} is the sub-grid scale viscosity. The uncertainties in estimating the effective viscosity and the turbulent flame speed are compensated by varying the C coefficient for different cases.

RESULTS AND DISCUSSIONS

The velocity profile at the location of the perforated-plate/swirler-vanes should be set as boundary condition but this profile is not available from the experiment. Therefore, based on the total burner mass flow and the measured velocity profile 10mm downstream of the burner exit, several candidate velocity profiles are imposed at this inflow

boundary in order to find the correct boundary conditions (Irannezhad and Eriksson, 2008). These profiles give a range of different swirl numbers. In a narrow range of swirl numbers the core flow is decelerated enough to let the flame stabilize and yet no strong recirculation zone is created; which characterizes the low swirl burner operating conditions.

The candidate profiles are used as boundary conditions in the coarse grid simulations in order to reduce the computational time. The computed flow for the chosen inlet profile is shown in figures 5 and 6 as radial profiles of mean velocity components at different distances from the burner exit.

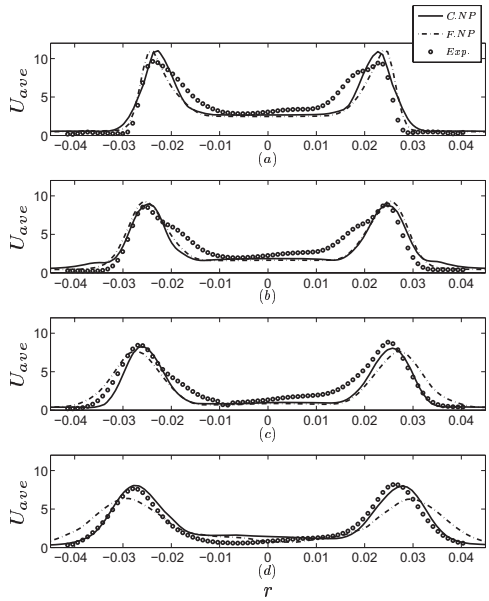

Figure 5: Radial profiles of the mean axial velocity at 10mm(a), 20mm(b), 30mm(c) and 40mm(d) downstream of the burner exit. Legend bar key: $C.NP$ refers to coarse grid simulations, $F.NP$ refers to fine grid simulations without the perforated plate and $Exp.$ refers to experimental data.

The flow compares well with the experimental data specially at 10mm downstream of the burner exit which has been used as the main criterion in selecting among the candidate profiles. This good comparison indicates that the choice of the inflow boundary condition profile is reasonable. This profile is then used in the fine grid simulations and the computed flow exhibits good comparison at 10mm downstream of the burner exit as shown in figures 5 and 6. Therefore, the same inlet profile was used for further simulations. The temperature profiles exhibit some discrepancy from the experimental data. The coarse grid results in the correct positioning of the flame but the flame is thin compared to the experimental observations. The fine grid flame is thicker but there exists a hole in the core region which persists a distance from the flame front in the shear layer.

FLAME STABILIZATION

The stabilization mechanism of this kind of flames is not yet well understood. Cheng et al.(2000) suggests that the core flow is decelerated by the act of the divergent swirling flow to match the local flame speed at some point where the flame can sit. Nogenmyr (2008) showed that the flow velocity in the shear layer around the core flow is much higher than the local flame speed. He suggests that the flame in

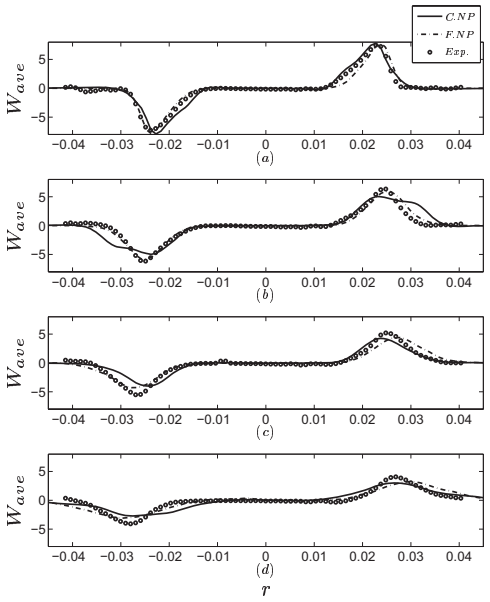

Figure 6: Radial profiles of the mean tangential velocity at 10mm(a), 20mm(b), 30mm(c) and 40mm(d) downstream of the burner exit. Legend bar key: as figure 5.

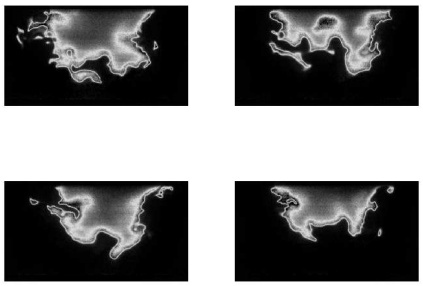

Figure 7: Flame front structure in real flame visualized by simultaneous fuel PLIF and OH PLIF images.

the shear layer is stabilized by the act of vortex rings and the flame at the core region is sustained by the large structures continuously shifting the flame toward the shear layer making V and W shaped flames.
Figure 7 shows snapshots of the flame front structures in the real flame where the flame exhibits highly dynamic behavior and wrinkling both in the core and in the shear layer regions. The aforementioned V and W shaped are also visible in this figure.

Figures 8 and 9 show snapshots of the flame front in both coarse and fine grid simulations. The coarse grid simulations show a rather flat flame front in the core region and the fine grid simulations ,though showing slight dynamics in the core region, is very calm compared to the experimental snapshots. There exists a hole in the core of the flame front in fine grid simulations which manifests itself as a hole in radial profile of the mean temperature. The cause of this discrepancy in flame front dynamics may be explained by the act of the large structures produced as a result of the jets emanating from the holes of the perforated plate. Figures 10, 11 and 12 compare the rms values of different velocity components of the simulations with the experimental data.

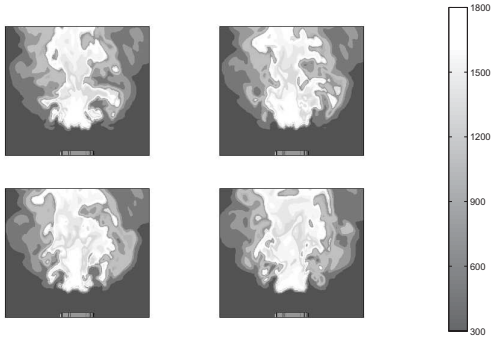

Figure 8: Flame front structure in coarse grid simulations visualized by temperature contours at the center plane.

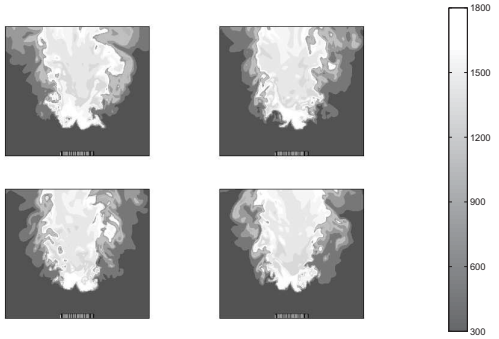

Figure 9: Flame front structure in fine grid simulations without the perforated plate visualized by temperature contours at the center plane.

The computed flows look laminar in the core region while the experimental data shows rms values for different velocity components which are of the order of the laminar flame speed of the mixture ($S_L = 0.13m/s$ for methane at the equivalence ration of 0.62). These large variation of velocity specially in the radial direction can move the flame within the core region and create the dynamics and flame wrinkling observed in the experiment.

PERFORATED PLATE SIMULATION

In order to generate these large structures in the core region, the computational domain is extended back to the perforated plate which is simulated as 37 separate jets in accordance to the 37 holes in the real perforated plate. This extension is only at the perforated plate region and the swirler vanes are not yet included in the computational domain. The dark area in figure 4 shows the part which is added to the domain and figure 13 shows how the boundary condition is set at the perforated plate as regions of high velocity resembling the holes and regions of zero velocity showing the wall part of the plate. Introducing the holes to the simulations affects the swirl number which should be adjusted for the new boundary condition applied which is done by changing the swirler vane angle.

Figure 14 shows the resulting flame front structures at several snapshots which indicates that the addition of the holes results in a highly dynamic flame front at the core region.

The radial profiles of mean and rms velocity components

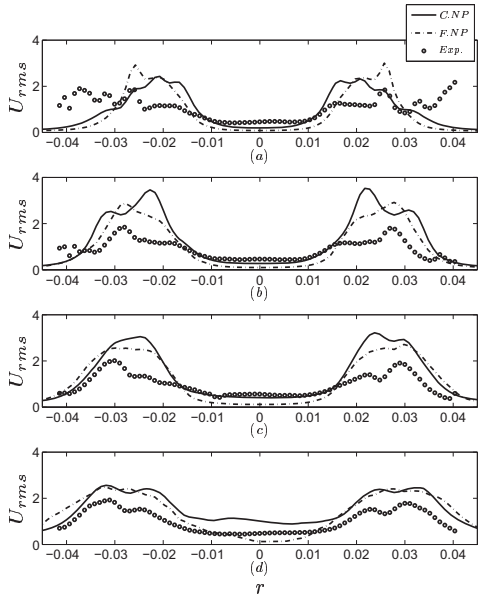

Figure 10: Radial profiles of the rms axial velocity at 10mm(a), 20mm(b), 30mm(c) and 40mm(d) downstream of the burner exit. Legend bar key: as figure5.

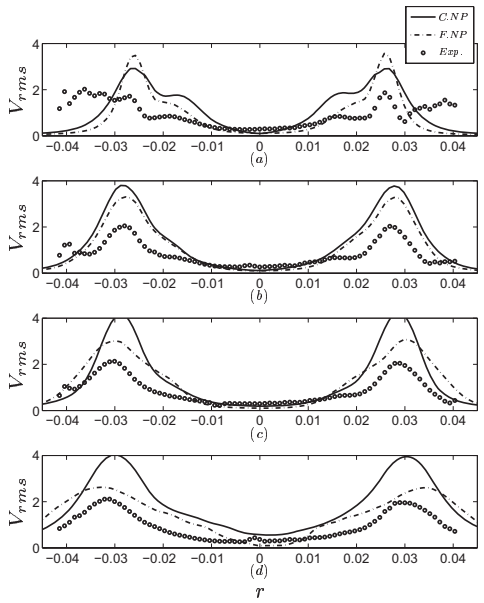

Figure 11: Radial profiles of the rms radial velocity at 10mm(a), 20mm(b), 30mm(c) and 40mm(d) downstream of the burner exit. Legend bar key: as figure 5.

for this case are compared to the fine mesh simulations and experimental data in figures 15-19.

The rms values show that the required turbulence in the core region is generated by the act of the added jets. The computed flame well resembles the real flame but is located at a farther distance from the burner exit compared to the real flame. The mean axial velocity does not compare well with the experimental data specially at the core region.

CONCLUSIONS

The results reveal that large eddy simulation with flame

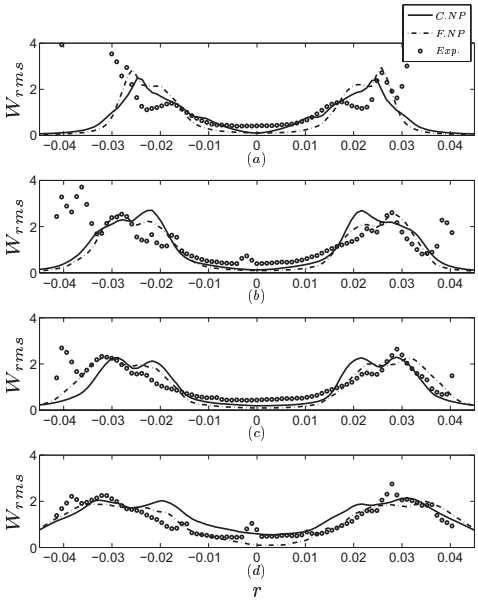

Figure 12: Radial profiles of the tangential rms velocity at 10mm(a), 20mm(b), 30mm(c) and 40mm(d) downstream of the burner exit. Legend bar key: as figure 5.

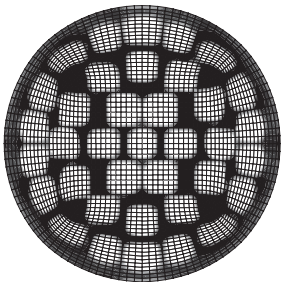

Figure 13: The velocity contours at the perforated plate location showing the holes as regions of high velocity. The grid lines represent the real grid lines.

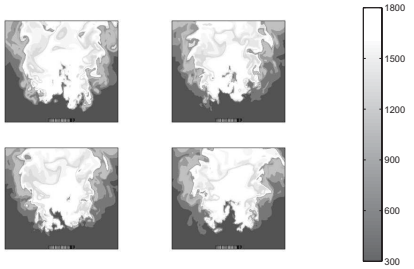

Figure 14: Flame front structure in fine grid simulations including the perforated plate visualized by temperature contours at the center plane

capturing combustion model can predict the flame dynamics and instabilities associated with them. The turbulence generated at the perforated plate plays a major role in formation of the dynamic flame and its regeneration at the inlet is essential for numerical simulations.

The swirl number plays a central role in formation and breakdown process of vortical structures inside the burner nozzle (Irannezhad and Eriksson, 2008). This suggests that

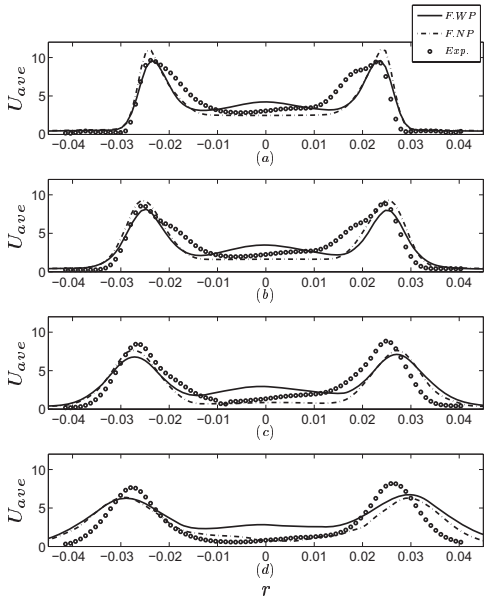

Figure 15: Radial profiles of the mean axial velocity at 10mm(a), 20mm(b), 30mm(c) and 40mm(d) downstream of the burner exit. Legend bar key: $F.WP$ refers to fine grid simulations with the perforated plate, $F.NP$ refers to fine grid simulations without the perforated plate and $Exp.$ refers to experimental data.

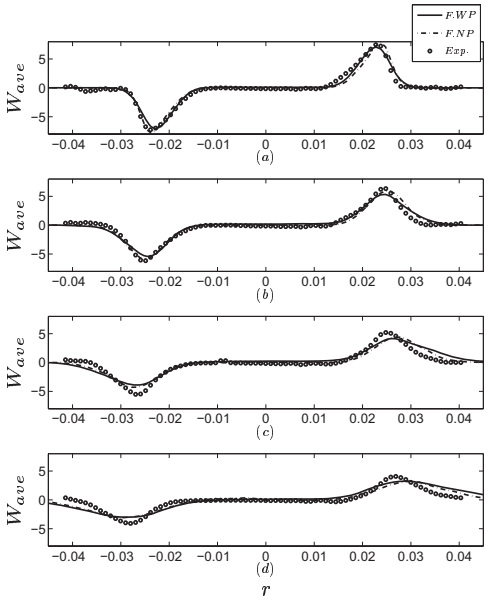

Figure 16: Radial profiles of the mean tangential velocity at 10mm(a), 20mm(b), 30mm(c) and 40mm(d) downstream of the burner exit. Legend bar key: as figure 15.

this flow and the corresponding flame structure is sensitive to the swirl number which is not known from experiments. Moreover, the inlet mass flow ratio split between the perforated plate and swirler vanes is not known. Both these important parameters are guessed when setting the inlet boundary condition and may not exactly correspond to the experimental values which may explain part of the discrepancy seen in the computed flow compared to the experimental data.

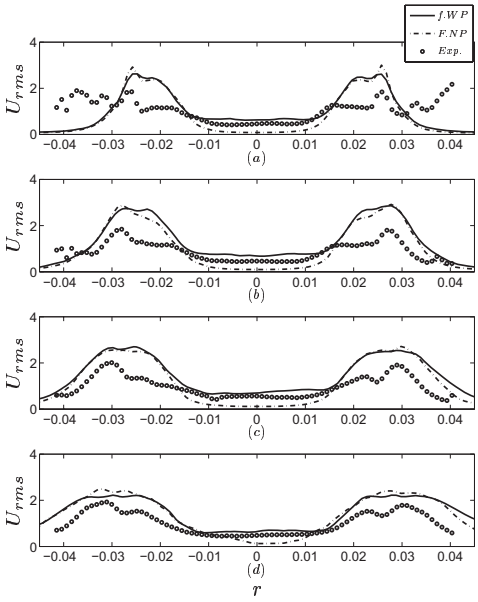

Figure 17: Radial profiles of the axial rms velocity at 10mm(a), 20mm(b), 30mm(c) and 40mm(d) downstream of the burner exit. Legend bar key: as figure 15.

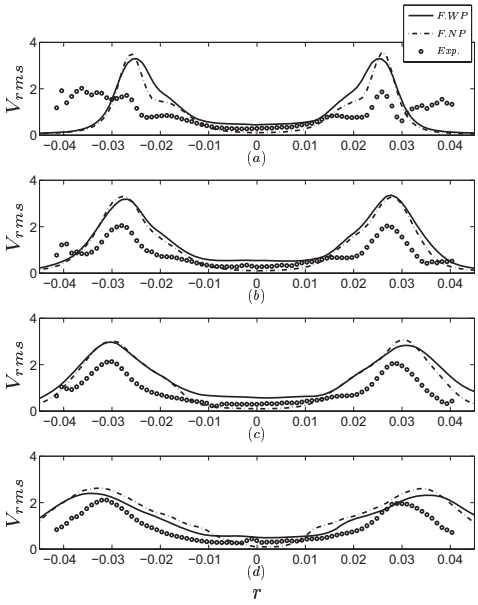

Figure 18: Radial profiles of the radial rms velocity at 10mm(a), 20mm(b), 30mm(c) and 40mm(d) downstream of the burner exit. Legend bar key: as figure 15.

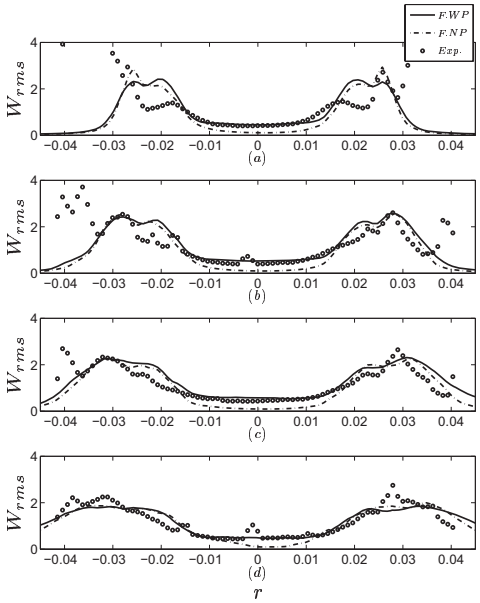

Figure 19: Radial profiles of the tangential rms velocity at 10mm(a), 20mm(b), 30mm(c) and 40mm(d) downstream of the burner exit. Legend bar key: as figure 15.

REFERENCES

Andersson, N., Eriksson, L.-E., and Davidson, L., 2005, "Large Eddy Simulation of Subsonic Turbulent Jets and Their Radiated sound",*AIAA Journal*, Vol. 43, pp. 1899-1912.

Bedát, B., and Cheng, R. K., 1995, "Experimental Study of Premixed Flames in Intense Isotropic Turbulence", *Combustion and Flame*, Vol. 100, pp. 485-494.

Cheng, R. K., Yegian, D. T., Miyasato, M. M., Samuelsen, G. S., Benson, C. E., Pellizzari, R., and Loftus, P., 2000, "Scaling and Development of Low-Swirl Burners for Low-Emission Furnaces and Boilers", *Proceedings of the Combustion Institute*, Vol. 28, pp. 1305-1313.

Clavin, P., and Williams, F. A., 1979, "Theory of Premixed-Flame Propagation in Large Scale Turbulence", *Journal of Fluid Mechanics*, Vol. 90, pp. 589-604.

Eriksson, L.-E, 1996, "A Preconditioned Navier-Stokes Solver for Low Mach Number Flows", *proceedings, Third ECCOMAS Computational Fluid Dynamics Conference*, Paris, France.

Irannezhad, M., and Eriksson, L.-E., 2007, "Flow-Flame Interactions in a Lean Premixed Low Swirl Burner", *Proceedings, 7th International Symposium on Engineering Turbulence Modeling and Measurements-ETMM7*, Vol. 3, pp. 690-694.

Johnson, M. R., Littlejohn, D., Nazeer, W. A., Smith, K. O., and Cheng, R.K., 2005, "A Comparison of the Flow fields and Emissions of High-Swirl Injectors and Low-Swirl Injectors for Lean Premixed Gas Turbines", *Proceedings of the Combustion Institute*, Vol. 30, pp. 2867-2874.

Kang, D. M., Culick, F. E. C., and Ratner, A., 2007, "Combustion Dynamics of a Low-Swirl Combustor", *Combustion and Flame*, Vol. 151, pp. 412-425.

Littlejohn, D., and Cheng, R. K., 2007, "Effects of Flames Stretch and Wrinkling on CO Formation in Turbulent Premixed Combustion", *Proceedings of the Combustion Institute*, Vol. 29, 1873-1879.

Nogenmyr, K.-J, 2008, "On the Modeling of Premixed Combustion under Varying Equivalence Ratios", Ph.D. Thesis, Division of Fluid Mechanics, Lund University, Lund.

Petersson, P., Olofsson, J., Brackman, C., Seyfried, H., Zetterberg, J., Richter, M., Aldeń, M., Linne, M. A., Cheng, R. K., Nauert, A., Geyer, D., and Dreizler, A., 2007, "Simultaneous PIV/OH-PLIF,Rayleigh thermometry/OH-PLIF and stereo PIV measurements in a low-swirl flame", *Applied Optics*, Vol. 46, pp. 3928-3936.

Shepherd, I. G., Cheng, R. K., Plessing, T., Kortschick, C., and Peters, N., 2002, "Premixed Flame Front Structure In Intense Turbulence", *Proceedings of the Combustion Institute*, Vol. 29, pp. 1833-1840.